ACS OMEGA

Open Access

http://pubs.acs.org/journal/acsodf

Article

L-Cysteine-Modified Carbon Dots Derived from *Hibiscus rosa-sinensis* for Thiram Pesticides Identification on Edible Perilla Leaves

Tanima Bhattacharya, Rahul Joshi, Lemma Teshome Tufa, Mahendra Goddati, Jaebeom Lee, Ameeta Tewari, and Byoung-Kwan Cho*

Cite This: *ACS Omega* 2024, 9, 47647−47660

Read Online

ACCESS | Metrics & More | Article Recommendations

ABSTRACT: In this work, environmentally friendly fluorescent carbon dots (C-dots) were developed for the purpose of thiram identification in the leaves of perilla plants. Powdered plant petals from *Hibiscus rosa-sinensis* were hydrothermally combined to create C-dots. Analytical techniques, such as scanning electron microscopy, energy dispersive X-ray spectroscopy, high resolution transmission electron microscopy, Raman spectroscopy, ultraviolet spectroscopy, Fourier transmission infrared spectroscopy, and photoluminescence were employed to examine the properties of C-dots. To enhance their functionality, an L-cysteine dopant was added to the C-dots. Since this process produces highly soluble C-dots in water, it is simple, inexpensive, and safe. The excitation process and the size of the blue luminescent C-dots both affect their photoluminescent activity. Furthermore, thiram in aqueous solutions was effectively identified by using the generated C-dots. Additionally, the ImageJ program was used to measure the colors red, green, and blue. High-resolution TEM (HR-TEM) revealed that the L-cysteine-doped carbon dots had an average particle size of 2.208 nm. Additionally, the lattice fringes observed in the HRTEM image showed a *d*-spacing of around 0.285 nm, which nearly corresponds to the (100) lattice plane of graphitic carbon. A Raman spectrum study was also performed to investigate the relationship between carbon dots and pesticides in the actual samples. In the end, thiram levels in perilla leaves with nondoped and doped C-dots could be distinguished with 100% accuracy using the constructed partial least-squares discriminant analysis machine learning model. The information gathered therefore demonstrated that the synthetic C-dots successfully and efficiently provide rapid and sensitive detection of hazardous pesticides in edible plant products.

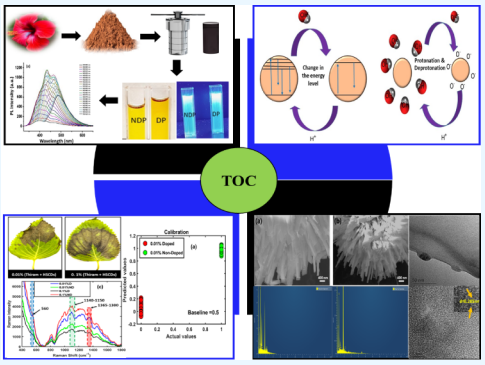

1. INTRODUCTION

Carbon dots (C-dots) have emerged as promising research topics in the field of carbon nanomaterials. They possess unique properties, such as solubility, low toxicity, and biocompatibility, making them attractive as semiconductor quantum dots.[1] Researchers are particularly interested in their fluorescent and photoluminescent properties, which are responsible for their applications in various fields, including biomedicine, catalysis and sensing, cell imaging, fluorescent staining, and demonstration.[2]

Different methods can be used to fabricate carbon dots, such as hydrothermal[3] and solvothermal carbonization of organic compounds, laser ablation,[4] ultrasonication, and microwave pyrolysis.[5] Among these methods, hydrothermal condensation is preferred because of its simplicity, directness, and ease of use. An attractive feature of the hydrothermal process is that it does not require strong acids or postsynthetic surface passivation when the starting materials are derived from natural sources.[6] Hydrothermal carbonization is a valuable method known for its favorable reaction conditions and minimal use of chemicals to produce fluorescent carbon dots.[7] Recently, biosynthesis methods have gained attention for producing nanosized materials from natural sources, such as chestnuts,[8] coriander,[9] lemon peel,[10] cashew gum,[11] honey,[12] orange juice,[13] orange peels,[14] radishes,[15] eggs,[16] shrimp,[16] pitahaya,[17] milk,[18] apple juice,[19] the stems of banana peels,[20] pineapple peel,[21] rose flowers,[22] and more. These methods offer alternatives to high-cost synthesis methods and utilize readily available resources. This study presents a straightforward, cost-effective, and environmentally friendly approach to synthesize C-dots using the petal powder of *Hibiscus rosa-sinensis* through a hydrothermal method.[23]

Carbon dots are preferred for insecticide sensing owing to their short analysis time,[24] low power consumption,[25] high sensitivity,[26] and ease of adaptation.[27] The remarkable sensing

Received: August 1, 2024
Revised: October 20, 2024
Accepted: November 5, 2024
Published: November 21, 2024

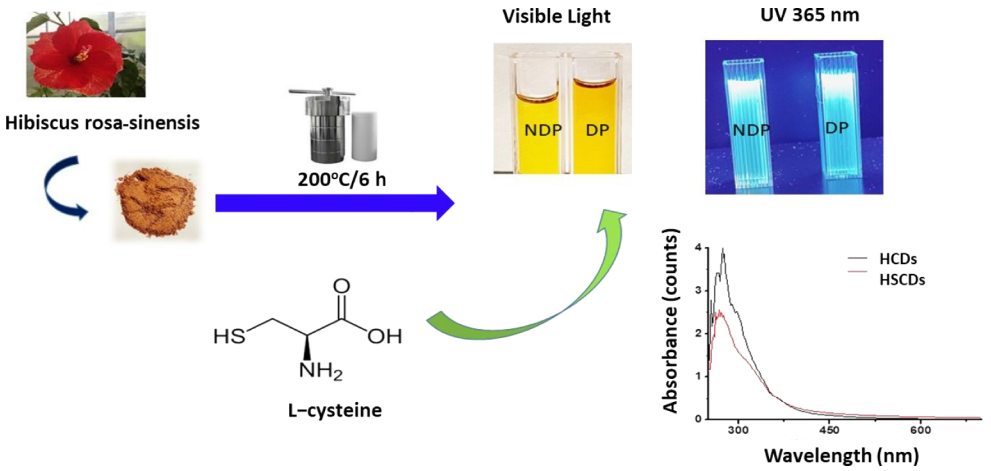

Figure 1. Schematic representation of carbon dot synthesis via a hydrothermal method—NDP, DP. Here NDP (non-doped), and DP (doped).

capability of the C-dots makes them promising candidates for detecting insecticides that are highly toxic and pose hazards to the environment and agricultural life.[28] C-dots demonstrate high sensitivity and selectivity toward various insecticides.[29] Because thiram ions have detrimental effects on human health, it is crucial to develop simple, sensitive, and accurate methods for their detection in the environment and food. In addition, the size, fluorescence, and luminescence properties of C-dots make them suitable for use as heavy metal sensors.[30] The developed C-dots serve as sensors for heavy metals, such as Ag^+ ions, significantly enhancing the device performance in terms of sensitivity, selectivity, multiplexed detection capability, and portability.[30]

In recent times, the use of carbon dots for real sample analysis[31] has gained significant attention within the material science community. Given the context of South Korea, the research team selected Perilla leaves, one of the most commonly consumed salad greens among Koreans,[32] as their real sample. The widespread misuse of pesticides[33] during the cultivation of agricultural products like Perilla poses a significant risk. Perilla has been widely used as both a traditional medicine and functional food in Asian communities.[34] It is used to treat various conditions, such as depression-related diseases, asthma, anxiety, tumors, coughs, allergies, intoxication, colds, fever, chills, headaches, stuffy nose, and certain intestinal disorders. Additionally, its attractive appearance and morphological variability make it a popular ornamental plant in gardens. Perilla is also used in culinary applications, including salads, sushi, and soups, and as a spice, garnish, or food colorant. Its seed oil has been traditionally used for flavoring foods.[35] Beyond its medicinal and culinary uses, perilla has gained importance in the cosmetics industry, where it is processed into skin creams, soaps, and dermatological preparations owing to its biological activities.[36]

Therefore, this research group aimed to address the real-world challenge of detecting pesticide residues in Perilla by utilizing carbon dots as sensors. In this study, the researchers employed heteroatom-doped carbon dots synthesized from *Hibiscus rosa-sinensis* petal powder. L-cysteine was selected as the functional agent or dopant[37] due to its sulfur and amino groups. Previous studies have shown that these groups can significantly enhance the functional properties of carbon dots, ensuring strong fluorescence[38] and stability,[39] which are crucial for the accurate detection of fungicides in real-life samples.[40]

Raman spectroscopy is a highly sensitive, nondestructive evaluation technique used for analytical purposes. This type of spectroscopy is popular in the field of carbon dot characterization. For example, Atchudan et al.[41] used dwarf banana peels to synthesize hydrophilic nitrogen-doped carbon dots from biowaste for environmental and biological applications, and the graphitization of the produced hydrophilic nitrogen-doped carbon dots (HN-CDs) was confirmed by Raman spectroscopy. On the other hand, Sarkar et al.[42] used Raman spectroscopy as a characterization method related to the D-band and G-band at 1352 and 1607 cm^{-1} during the examination of vitamin D from carbon dot-modified chitosan. Further, in a previous study, Ashrafi Tafreshi et al.[31] performed ultrasensitive fluorescent detection of pesticides in a real sample by using green carbon dots with a detection limit of 0.25, 0.5, and 2 ng mL^{-1} for diazinon, amicarbazone, and glyphosate, respectively. In this study, we demonstrate that C-dots derived from *Hibiscus rosa-sinensis* can serve as potent fluorescent probes for sensing thiram ions. The sensitivity of fluorescent C-dots toward thiram ions in aqueous solutions was investigated using Raman spectroscopy technique coupled with popular machine learning method, namely, partial least-squares discriminant analysis for the discrimination of higher and lower thiram insecticide concentrations on perilla leaves infected with non-doped carbon dots (HCDs) and doped carbon dots (HSCDs). The one-step, cost-effective synthesis of carbon dots through the hydrothermal method, utilizing the easily available natural source *Hibiscus rosa-sinensis*, motivated us to choose this approach for C-dot preparation. The carbon dots are prepared by dehydration, and carbonization mechanism.[43] As per our knowledge, this study is the first study of detection of thiram in perilla leaves as real sample analysis using a machine learning approach.

2. MATERIALS AND METHODS

2.1. Materials. The local market provided dried Hibiscus flowers, which were acquired without any prewashing. The samples were dried and crushed into powder to retain all of the organic compounds and enhance surface functionalization. Distilled water was used as the dispersant. A Whatman filter paper with a pore diameter of 0.22 μm was used to obtain carbon quantum dots (CQDs). L-cysteine was purchased from Sigma-Aldrich (St. Louis, MO, USA) and Thiram was purchased from Sigma-Aldrich (Germany).

https://doi.org/10.1021/acsomega.4c07090
ACS Omega 2024, 9, 47647−47660

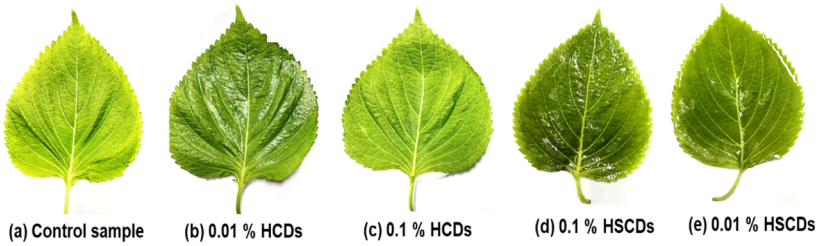

Figure 2. Control sample of the perilla leaf without any contamination (a). Thiram insecticide-infected perilla leaves (0.1% and 0.1%, concentrations) (b,c) were used for HCD samples. HSCD samples were sprayed on perilla leaves that are infected with thiram with 0.1% and 0.01% concentrations (d,e). HCD, non-doped carbon dots; HSCD, doped carbon dots. The reported leaves picture was taken at 0 h of the treatment.

2.2. Synthesis of Carbon Dots. A one-pot hydrothermal method was employed to produce carbon quantum dots (HCDs) using *Hibiscus rosa-sinensis*. First, 1 g of dried petal powder was combined with 50 mL of distilled water in a Teflon-lined stainless-steel reactor with a capacity of 100 mL. The mixture was then heated by hydrothermal synthesis at 200 °C for a duration of 6 h[44] as shown in Figure 1. After the reaction, the solution was allowed to cool, and the solid portion was separated by centrifugation at 8000 rpm for 30 min. The resulting supernatant was filtered through a 25 mm diameter Whatman membrane filter with a pore size of 0.22 μm from Whatman International Ltd., Maidstone, UK to eliminate impurities.

Sulfur amino acid-doped petal powder carbon dots (HSCDs) were simultaneously synthesized. This was achieved by adding 0.5 g of L-cysteine amino acid to 1 g of petal powder prior to the hydrothermal synthesis at a temperature of 200 °C for 6 h. But in the present case, centrifugation was used to separate the solid portion of the carbon dots that were produced, and it was done for 15 min at a speed of 10,000 rpm. Similar Whatman membrane filters with a 25 mm diameter and 0.22 pore size were employed in the filtration process to remove undesired contaminants.

2.3. Sample Preparation for Thiram Concentration. In this study, thiram was produced in a total volume of 30 mL using two separate concentrations (0.01% and 0.1%). Methyl alcohol was used as the solvent. Following sample preparation, a homogeneous solution was created by uniformly combining the components by using a vortex vibration machine. The mixing process was performed in a chemical fume hood to ensure chemical safety. In addition, two different concentrations of pesticide-infected perilla leaves were sprayed with HSCDs or undoped HCDs. The perilla leaves shown in Figure 2b,c was only thiram-infected at concentrations of 0.01% and 0.1%, respectively, whereas the perilla leaves in Figure 2d,e had both doped and non-doped CDs sprayed on them. A control sample of perilla leaves without impurities is shown in Figure 2a.

2.4. Instrumentation and Characterization. The prepared carbon dots were analyzed using a PerkinElmer (Massachusetts, USA, Bruker ALPHA-P spectrophotometer) to obtain FTIR spectra. The surface zeta potential was monitored by using a ZS Nano Zetasizer (Malvern Instruments, Malvern, U.K.). The light absorbance of the HCDs was measured using a UV−vis spectrophotometer in the wavelength range of 280−600 nm. Specifically, a Mecasys Optizen POP Series UV/vis spectrophotometer (Seoul, Republic of Korea) was utilized for this purpose. To evaluate the absorbance and fluorescence spectra of the pristine and functionalized C-dots, photoluminescence (PL) spectra were recorded by using a MRRAY UV spectrophotometer (S310, SINCO Inc., Daejeon Sinco, Korea) and a fluorescence spectrophotometer (FS-2, Scinco, South KoreaF-7000, Hitachi, Japan) equipped with a quartz cuvette. Fluorescence measurements were performed for both the HCDs and sulfur-doped HCDs (HSCDs). The excitation power was adjusted to ensure comparability of the emission intensities. Excitation−emission scans were conducted at 20 nm increments in the excitation wavelength. Morphological analysis of the CDs was performed using field-emission scanning electron microscopy (FE-SEM, Merlin Compact, Carl Zeiss, Germany), followed by elemental composition analysis using energy-dispersive X-ray spectroscopy (EDS or EDX, FE-SEM Merlin Compact, Carl Zeiss). A portable i-Raman spectrometer (BWTEK Inc., USA) equipped with a 14 × 900 m charge-coupled device (CCD) detector and a 785 nm laser was used to record the Raman spectra of infected perilla leaves. Using a laser light source with a wavelength of 785 nm and a power of 200 mW, spectra were obtained for each sample at a spectral resolution of 2 cm^{-1} and an exposure period of 2 s. The particle size analysis and lattice parameter measurement were performed by Transmission Electron Microscopy (FEI Tecnai G2 F30).

2.5. Partial Least-Squares Discriminant Analysis Model. PLS-DA is a preferred machine learning method used for classification problems. It is a supervised approach mostly employed for group discrimination within different classes with distinctive characteristics.[45] It is regarded as an improved version of the partial least-squares regression (PLSR) method, in which partial least-squares (PLS) is employed as a criterion to obtain classification results. In this study, doped carbon dots were discriminated from a non−doped one using this method. In the PLS-DA model, the response variable Y has binary values representing different sample groups or categories. eq 1 presents the PLS-DA formula as follows:

$$Y = X \times b + C \quad (1)$$

where X is the $a \times b$ matrix that holds the Raman spectra values for each concentration of the thiram insecticide in perilla leaves, b represents regression coefficient, and C symbolize error matrix. The spectral data for the pure and mixed thiram pesticide samples were found in matrix Y, whereas artificial values were found in matrix X for each thiram percentage range. Pure and spiked samples can only be appropriately classified based on the threshold values. A threshold value of 0.5 was used for the purposes of this study, indicating that samples lying inside the 0.5 range are classified.[46]

https://doi.org/10.1021/acsomega.4c07090
ACS Omega 2024, 9, 47647−47660

2.6. Statistical Analysis. We measured newly prepared samples three times and reported the outcomes as mean ± standard deviation. Statistical analysis was performed using one-way analysis of variance (ANOVA) on a randomly arranged experimental design with SPSS software (SPSS Inc., Chicago, IL, USA). To distinguish differences among the test groups, Duncan's multiple range test ($p < 0.05$) was employed.

3. RESULTS AND DISCUSSION

3.1. Optical Properties. The water dispersion of HCDs and HSCDs, prepared by subjecting them to a temperature of 200 °C for 6 h with a L-cysteine concentration of 0.5 g/50 mL, exhibited blue emission when exposed to near-ultraviolet (UV) light at 365 nm.

The main components identified in *Hibiscus rosa-sinensis* include flavones, such as quercetin-3-sophorotrioside, kaempferol-3-xylosylglucoside, quercetin-3-diglucoside, quercetin-3,7-diglucoside, cyanidin-3,5-diglucoside, and cyanidin-3-sophoroside-5-glucoside. Additionally, other constituents include cyanidin chloride, cyclopeptide alkaloid, ascorbic acid, riboflavin, thiamine, hentriacontane, taraxeryl acetate, β-sitosterol, malvalic acids, and steric cyclic acids. These molecules undergo carbonization through hydrolysis, dehydration, and decomposition, followed by polymerization, condensation, and cycloaddition reactions, which ultimately generate the carbon core. This core is then passivated and functionalized, leading to the formation of CQDs. Similar mechanisms of formation of carbon dots was observed when rose petals were pyrolised at 180 °C for 5 h by Sharma et al.[47] Carbonization of polysaccharides and other constituents results in the creation of carbon dots from rose petals. PXRD (sp^2 carbon), ATR (−NH, C═N, C−N bonds), XPS (N 1*s* peak at 400.02 eV), and elemental analysis demonstrating variable C/N ratios all confirm this mechanism. The hydrolysis and dehydration of petal components during hydrothermal treatment yield C5 and C6 sugars and furans, such as 5-hydroxymethyl furfural and furfural. The study also revealed that cytosteine aids in acid hydrolysis, while ethylenediamine promotes dehydration of polysaccharides extracted from rose petals, as confirmed by various analytical techniques. This led to polymerization and polycondensation, forming nitrogen- and sulfur-containing aromatic clusters through aromatization and carbonization. These processes were verified by NMR (1D and 2D), ATR, UV−vis, and XPS analyses. Once the aromatic clusters reached a critical concentration, a nuclear burst occurred, resulting in the formation of N−S codoped carbon dots. In our case somewhat similar approach is considered as our *Hibiscus rosa-sinensis* is also doped with L-cysteine similar to Sharma et al. L-cysteine consists of both N and S groups as cysteine is sulfur consisting of amino acid. In our case, also the mechanism is relatable as that of Sharma et al. The synthesis of CQDs is primarily indicated by the color change of the extract dark brown solution and is confirmed by the visible blue fluorescence under UV light.[48,49]

The HCD dispersion emitted noticeably stronger blue light than the HSCD dispersion. Figure 3a,b shows the photoexcitation (PLE) and photoluminescence (PL) spectra of these dispersions. The HCD and HSCD dispersion exhibited the highest intensity at 365 and 385 nm, respectively, where bathochromic shifts were observed. These peaks correspond to transitions between π-levels and surface state levels as well as between π-levels and nitrogen-doped levels from L-cysteine amino acid. The PL quenching properties are prominent in the PL spectra of L-cysteine-modified hibiscus carbon dots owing to protonation and deprotonation when L-cysteine is added with *Hibiscus rosa-sinensis* petal powder phenomena, as shown in Figure 4. This quenching is supposed to happen due to interactions of oxygen containing functional groups from L-cysteine amino acid. Bao et al.[50] further discovered that the surface of carbon dots is covered with various functional groups, each affecting the properties of the carbon dots in different ways. Notably, some oxygen-containing functional groups can induce dynamic fluorescence quenching in carbon dots. Similar observations were made when copper-doped carbon dots were synthesized through direct pyrolysis, where no distinct photoluminescent properties were reported by Wu et al.[51] Wu et al. explained that these copper-doped carbon dots exhibited enhanced electron-accepting capabilities while also acting as electron donors, leading to an efficient quenching mechanism.

We also calculated the quantum yield of HCD to be 30%, whereas that of HSCD was 22%. From the UV−vis spectra, it

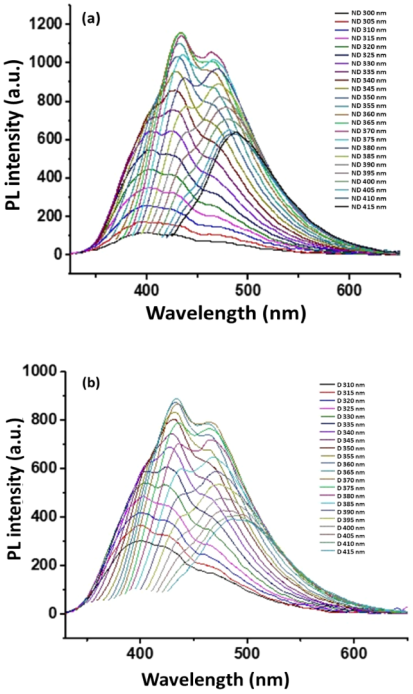

Figure 3. (a) HCD PL spectra. (b) HSCD PL spectra. PL, photoluminescence; HCD, non-doped carbon dots; HSCD, doped carbon dots.

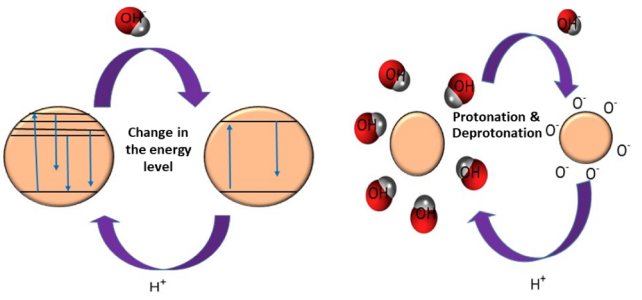

Figure 4. Deprotonation and protonation mechanisms of PL quenching of CDs. PL, photoluminescence; CDs, carbon dots.

https://doi.org/10.1021/acsomega.4c07090
ACS Omega 2024, 9, 47647−47660

Table 1. Comparison of QY of Different Carbon Dots Reported in Previous Studies

Name of Source	Technique	Dopant Used	*QY* (%)	References
Hibiscus rosa-sinensis	Hydrothermal	L-Cysteine	22	Present work
Hibiscus rosa-sinensis	Hydrothermal	-	30	Present work
Sugar cane industrial solid waste	Hydrothermal	Citric acid	17.98	55
Whole meal bread + soya flour + lemon juice	Sonication followed by centrifuge process	-	2.3	56
Human hair	Hydrothermal	-	28	57
Biowaste lignin	Hydrothermal	-	3.4	58
Biowaste lignin	Hydrothermal	Amine	21.1	58
Quinoa Saponin	Hydrothermal	Ethanediamine	22.2	59
Mango Peel	Hydrothermal	-	8.5 ± 0.2	60
Waste Carbon Paper	Simple Synthetic Route	(3-Aminopropyl)triethoxsilane (APTES)	5.1%	61
Orange waste	Hydrothermal	Citric acid	11.37%	62

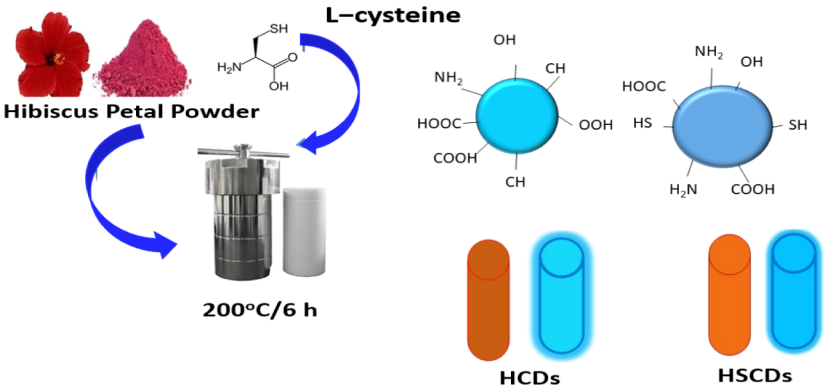

Figure 5. Surface functionalization of pristine CDs (carbon dots) with L-cysteine. HCD, nondoped carbon dots; HSCD, doped carbon dots.

was also noted that the L-cysteine-modified carbon dots (HSCDs) are more prone to UV barrier characteristics than pristine carbon dot HCDs. Our sample quantum yield is much better than that of previous reports on the quantum yield of biowaste-derived carbon dots, as summarized in Table 1. Atchudan et al. reported that almost an 18% quantum yield from kiwi fruit peel waste derived carbon dots was obtained using their synthesis technique[52] which they applied as bioimaging ink.

We noted in a very recent study that carbon dots synthesized from polypropylene, a common plastic, using the reprecipitation technique, exhibited a quantum yield ranging from 0.2% to 10%, depending on the variation in temperature conditions from low to high.[53] The quantum yield obtained in our case is compared with a study where Kumar et al. synthesized 20 sets of CDs from 20 coded commercially available amino acids. The average *QY* was 48%. Among which the cysteine derived carbon dots *QY* was 51%. From that detailed report it was observed that CDs derived from isoleucine, valine, leucine, and tyrosine had *QY* of 17%, 24%, 23%, and 16% respectively. The highest among them was arginine 86%.[54] We determined the relative quantum yield of C−dots by comparing them to that of Rhodamine 6G (*QY*: 94% at 480 nm). We used a 365 nm excitation wavelength and calculated the C−dot's quantum yield using the following formula:

$$QY = QY\left(ref\right)\left(\frac{A_s}{A_r}\right)\eta_s/\eta_{ref} \quad (2)$$

where *QY* represents the fluorescence quantum yield of the C-dot, *ref* is the reference quantum yield of R6G (0.94 at 480 nm excitation), η is the refractive index of the solvent, and *I* is the integrated fluorescence intensity. In our case, $\eta = \eta_{REF} = \eta_{WATER}$. A_s is the area of the slope for the sample and A_r is the area of the slope for the reference which was calculated by the software

3.2. FTIR. Figure 5 shows the surface functionalization steps of pristine carbon dots, which were later analyzed by using Fourier transform infrared (FT-IR) spectroscopy. Figure 6 represents the FTIR spectra of HCD and HSCD solution that were prepared by subjecting them to a temperature of 200 °C for 6 h with an L-cysteine concentration of 0.5 g/50 mL. In both samples, a broad peak ranging from 3200 to 3700 cm^{-1} was observed, which corresponded to the stretching vibrations of the O−H and amide N−H bonds. This suggests that an

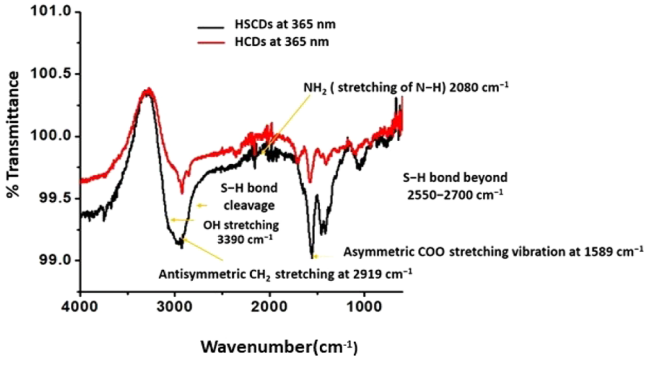

Figure 6. FTIR spectra were obtained to confirm the functional group presence. HCD, non-doped carbon dots; HSCD, doped carbon dots; FTIR, Fourier transform infrared.

https://doi.org/10.1021/acsomega.4c07090
ACS Omega 2024, 9, 47647−47660

intermolecular dehydration reaction between the carboxyl and amino groups in L-cysteine occurred in both samples, leading to the formation of amide bonds. In the region 2919 cm^{-1}, the antisymmetric CH_2 was more prominent in HSCDs than in HCDs. The combination band of asymmetric deformation and hindered rotation of NH_3^+ groups (protonated NH_2 groups) was observed in L-cysteine modified carbon dots, i.e., in the HSCD spectra but not in the HCD spectrum.[63] Consequently, the dehydration reaction was enhanced in the HSCDs, leading to the conversion of NH_2 to NH in the amide groups. In the 2080 cm^{-1} region, the stretching of NH_2 confirmed the L-cysteine functionalization of hibiscus carbon dots in a well-mannered way. S−H bond stretching is observed in HSCD in the 2050 cm^{-1} region but not in the HCD spectrum. Approximately 1450 cm^{-1} appeared in the spectra of both HCDs and HSCDs, indicating the stretching vibration of the C−N bonds formed through the dehydration reaction.[63] This suggests that dehydration occurred in both samples, resulting in the formation of amide bonds. Distinctive and well-defined peaks at 1589 cm^{-1} were observed in the spectrum of the HSCDs, confirming the presence of asymmetric COO^- stretching vibrations. This peak is attributed to the carbon−sulfur (C−S) bonds present in the compound. In HCDs, the dehydration reaction was more pronounced, resulting in a decrease in the proportion of NH_2 groups. This finding aligns with the results obtained from FT-IR analysis.

Moreover, the proportion of C−S bonds in the HSCDs was higher than that in the HCDs. This disparity can be attributed to the formation of volatile sulfur compounds through the pyrolysis of L-cysteine in an autoclave under aqueous solvent conditions, specifically for the synthesis of HSCDs.[64] However, such pyrolysis did not occur in the HCD solvent system used to produce the HCDs. We qualitatively detected the presence of volatile sulfur compounds based on their sulfurous odor after the preparation of HSCDs, whereas no such odor was detected in the HCD samples.

3.3. Colloidal Stability, Morphology, and Elemental Composition of HSCDs. The interaction between a nanoparticle and its surroundings is significantly affected by its surface charge.[65] The synthesized CDs contained functional groups, such as −COOH, −OH, and epoxides. These functional groups create electrostatic repulsion between CDs, preventing them from clumping together and allowing them to remain stable for several months.[65] All of the CDs derived from the hibiscus petal powder exhibited negative surface charges, indicating the presence of hydroxyl and carboxylate groups on their surfaces. The zeta potential values of the pristine and functionalized CDs were as follows (mean ± SD; mV): −2 ± 2.167 for pristine hibiscus CDs (HCDs) and −21.100 ± 1.197 for L-cysteine amino acid functionalized CDs (HSCDs) (Figure 7). Functionalization with sulfur amino acids was confirmed from our FTIR data, which was related to the negative surface charge of the HSCDs.

The structure of the materials was analyzed using a technique called field-emission scanning electron microscopy (FESEM). Figure 8a displays FESEM images of pristine carbon dots. Figure 8b shows the FESEM images of the HSCD composite material (L-cysteine-modified HCDs), while the results indicate the successful synthesis of a distinct and well-defined hierarchical rod like petaled flower nanostructure in the HSCDs. Each petal of the flower has a length of approximately 0.5 μm in the HSCDs composite. In contrast,

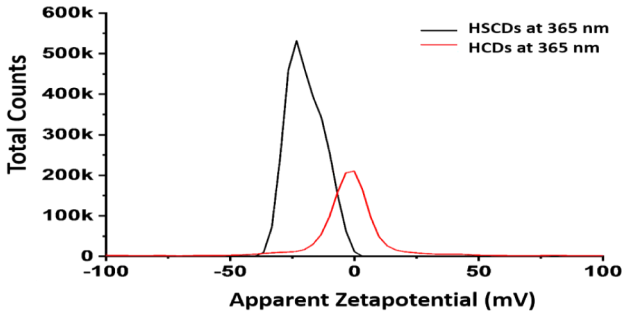

Figure 7. Zeta potential curves of HCDs and HSCDs. HCD, non-doped carbon dots; HSCD, doped carbon dots.

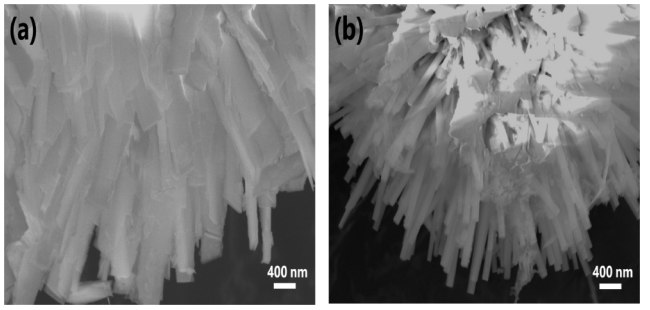

Figure 8. HCD SEM morphology (a) and HSCD SEM morphology (b). HCD, non-doped carbon dots; HSCD, doped carbon dots; SEM, scanning electron microscopy.

the SEM patterns of the HCDs differ from those of the composite material and exhibited overlapped rod like patterns.

Both forms have the same crystal structure, as was also observed in this study. The formation of HCDs occurs through a process known as diffusion-limited aggregation.[66] The presence of the C-dots is responsible for the formation of the overlapped rod morphology; HCDs were formed only when C-dots are present. In contrast, the rod like petaled flower morphology of HSCDs is formed through a mechanism called flake-cracking,[67] where the material initially takes on a sheet like shape, and then the flakes crack and, transform into nanorods. Moreover, carbon atoms may form continuous helical chains aligned parallel to the *c*-axis, bonded by covalent bonds, while these chains are arranged in a hexagonal lattice through van der Waals interactions. To promote the dominance of the stronger covalent bonds within the helical chains over the relatively weaker van der Waals forces between them, the growth rate along the direction should exceed that along the directions. This preference for crystallization and growth is observed during the biomolecule-assisted synthesis of carbon dots. Concurrently, the elevated reaction temperature intensifies the Brownian motion of the oxidized species, leading to the disruption of the weak van der Waals interactions. These factors cause the carbon dots to initially fracture into small nanobelts or nanowires at both ends, subsequently evolving into belt-like or wire-like patterns. However, there is limited documentation on the flake-cleavage mechanism nanomaterials in current methodologies. Therefore, our research may unveil a novel mechanism for synthesizing nanomaterials with an anisotropic structure. Based on experimental findings and discussions, a possible mechanism for the formation of carbon nanoribbons is proposed. However, further systematic investigation is warranted to gain a deeper understanding of the flake-cracking

https://doi.org/10.1021/acsomega.4c07090
ACS Omega 2024, 9, 47647−47660

mechanism of these nanomaterials, which is currently ongoing in our research group. Though flower shaped carbon dots morphological structure was reported by He et al.[68]

The phenomenon of flake-cracking has been observed in the synthesis of single-crystalline selenium nanowires and nanoribbons assisted by biomolecules[67] shown in Figure 9. The

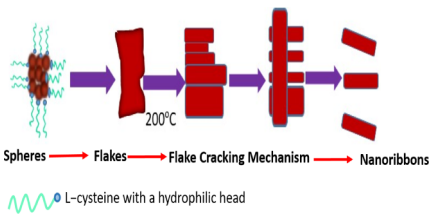

Figure 9. Flake cracking mechanism to transform into nanoribbons (to understand the morphology of carbon dots).

surface charge was very different between the two cases (−2 mV in the case of HCDs and −21 mV in the case of HSCDs).

From the EDX spectral analysis, we investigated the detailed elemental composition differences in the HCDs and HSCDs.

A Japanese group of professors provided an excellent review perspective, highlighting that quantum dots are unique among nanomaterials and are categorized into three nanosystems and one bulk system based on the number of dimensions with quantum confinements. These range from bulk materials with no quantum confinement (n = 3), to quantum wells or thin films with confinement in two dimensions (n = 2), quantum wires or nanotubes with one-dimensional confinement (n = 1), and quantum dots, which are nanoparticles confined in all three dimensions (n = 0).[69] Another group of reserachers engineered 2D triangular carbon dots and explained their applicability as multicolor Light emitting diode.[70] The present researchers' SEM analysis has also revealed wire-, rod-, and nanotube-like structures, indicating that the morphology of carbon quantum dots can exhibit various shapes beyond the typical spherical or quasi-spherical forms.

Further, EDX was used to examine the elemental composition of the samples. The results are listed in Figure 10. The analysis revealed that HCDs consisted solely of carbon

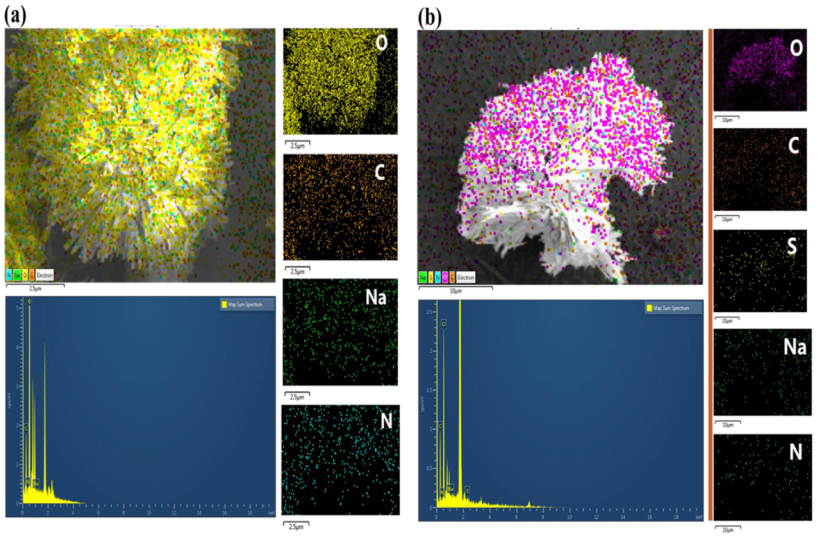

Map Sum Spectrum for HCDs (c)

Element	Line Type	Apparent Concentration	k Ratio	Wt%	Wt% Sigma	Atomic %
C	K series	11.37	0.11371	14.19	0.74	18.01
N	K series	7.47	0.01330	1.64	0.85	1.78
O	K series	222.30	0.74808	84.17	1.03	80.21
Na	K series	0.00	0.00000	0.00	0.59	0.00
Total:				100.00		100.00

Map Sum Spectrum for HSCDs (d)

Element	Line Type	Apparent Concentration	k Ratio	Wt%	Wt% Sigma	Atomic %
C	K series	8.72	0.08720	33.13	1.71	39.79
N	K series	2.05	0.00365	1.75	1.92	1.81
O	K series	50.88	0.17122	64.40	2.10	58.07
Na	K series	0.00	0.00000	0.00	0.81	0.00
S	K series	0.32	0.00271	0.72	1.10	0.33
Total:				100.00		100.00

Figure 10. (a) Composition elemental analysis of HCDs chart with distribution. (b) Composition elemental analysis of HSCDs chart with distribution. (c) Elements C, N, and Na peaks are prominent in HCDs in EDS report. (d) Elements C, N, Na, and extra S peaks are prominent in HSCDs in EDS report.

https://doi.org/10.1021/acsomega.4c07090
ACS Omega 2024, 9, 47647−47660

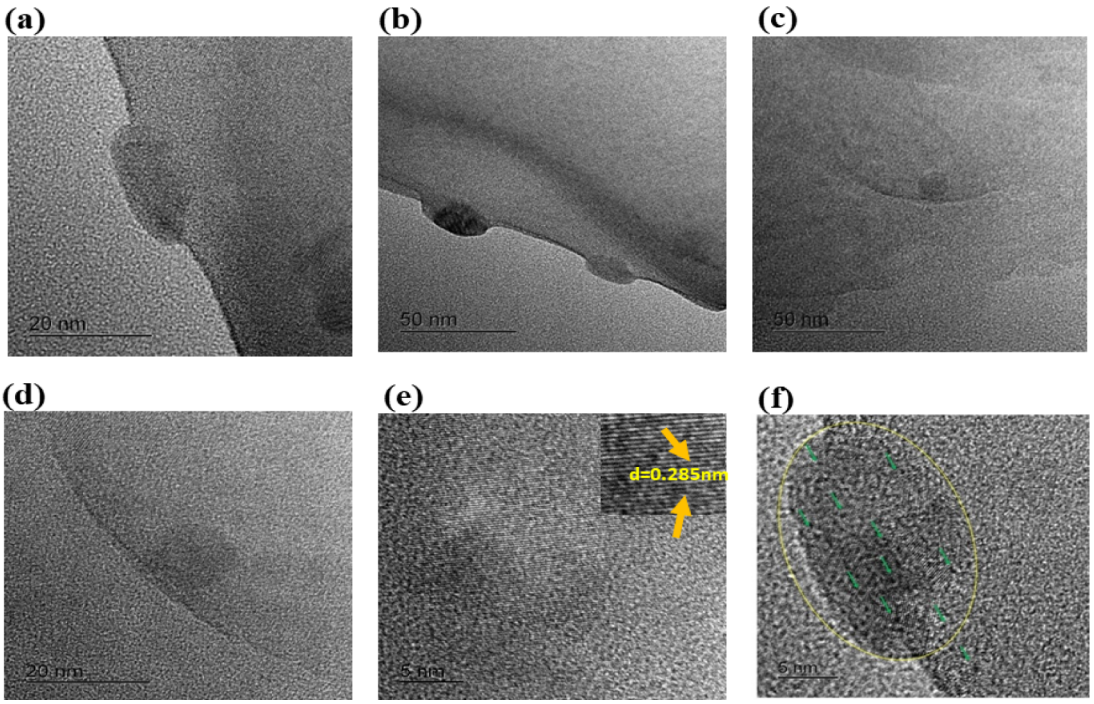

Figure 11. Carbon dot clusters containing HCDs and HSCDs are reported at different scale. (a) HCD at 20 nm scale (b) HCDs at 50 nm scale, (c) HSCD at 20 nm scale, (d) HSCD at 50 nm. (e) The lattice parameter is reported as d = 0.285 nm (The detailed calculation is done by ImageJ Software). The clusters magnified and each carbon dots are measure by ImageJ software, and average size of the particle is reported to be 3 nm. (f) The HSCD at 5 nm scale is reported, and green arrows highlight individual carbon dots in the cluster.

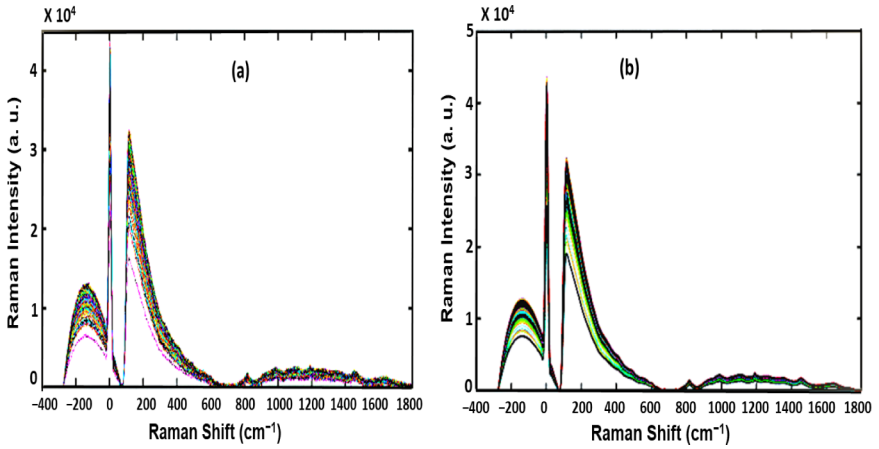

Figure 12. Original Raman spectra (a) and fluorescence-corrected Raman spectra using the polynomial curve fitting method (b) for doped samples.

(C), oxygen (O), nitrogen (N), and sodium (Na) shown in Figure 10a, whereas the HSCDs samples contained predominantly C, O, and sulfur (S) atoms shown in Figure 10b. This suggests that even after irradiation C and O atoms remained in the samples. The EDX spectra indicated the presence of Si in the substrate used in the experiment. The atomic percentages of C and O were 18.01% and 80.21% and 39.79% and 58.07% in the HCDs and HSCDs, respectively shown in Figure 10c,d. This indicated a reduction in the number of oxygen-containing functional groups on the surface of the HSCDs. Sulfur was also present in the samples with atomic percentages of 0.33% in the HSCDs, respectively. These findings confirmed the successful sulfur doping of HCDs with sulfur-containing cyclic L-cysteine amino acids. Das et al.[71] reported similar results.

3.4. Transmission Electron Microscopy (TEM). From Figure 11, High-resolution TEM (HR-TEM) revealed that the L-cysteine-doped carbon dots had an average particle size of approximately 2.208 nm. Additionally, the lattice fringes observed in the HRTEM image (Figure 11d) showed a d-spacing of around 0.285 nm, which nearly corresponds to the (100) lattice plane of graphitic carbon. However, the absence of the 0.33 nm spacing typical for the graphitic plane indicates that the L-cysteine-doped carbon dots' surfaces are coated with polar functional groups attached to aliphatic carbons such as amino acids. Similar reports are observed in Mohammed et al.,[72] where researchers observed lattice fringes in nitrogen-doped carbon dots, which had 0.26 nm d-spacing corresponding (100) lattice plane to graphitic carbon.

3.5. Raman Spectroscopy with Spectral Preprocessing, and Chemometrics Analysis. Raman spectra are commonly affected by background fluorescent signals, which obscure important data regarding the chemical structure of

https://doi.org/10.1021/acsomega.4c07090
ACS Omega 2024, 9, 47647−47660

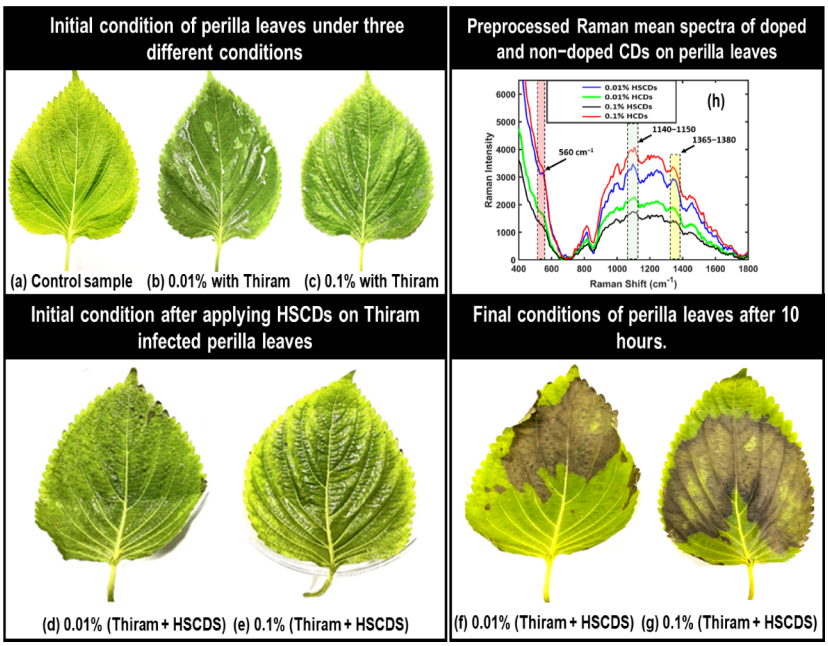

Figure 13. (a) Control perilla leaf sample. Perilla leaves with two different 0.01%, and 0.1% Thiram pesticides concentrations (b,c). Perilla leaves with both thiram and HSCDs (d,e). Visual appearance of doped CD (carbon dots) sprayed perilla leaves with (a) 0.01% thiram and (b) 0.1% thiram (f,g). Preprocessed Raman mean spectra (h) of doped and nondoped CDs on perilla leaves at two distinct concentrations of thiram (0.01% and 0.1%). HCD, nondoped carbon dots; HSCD, doped carbon dots.

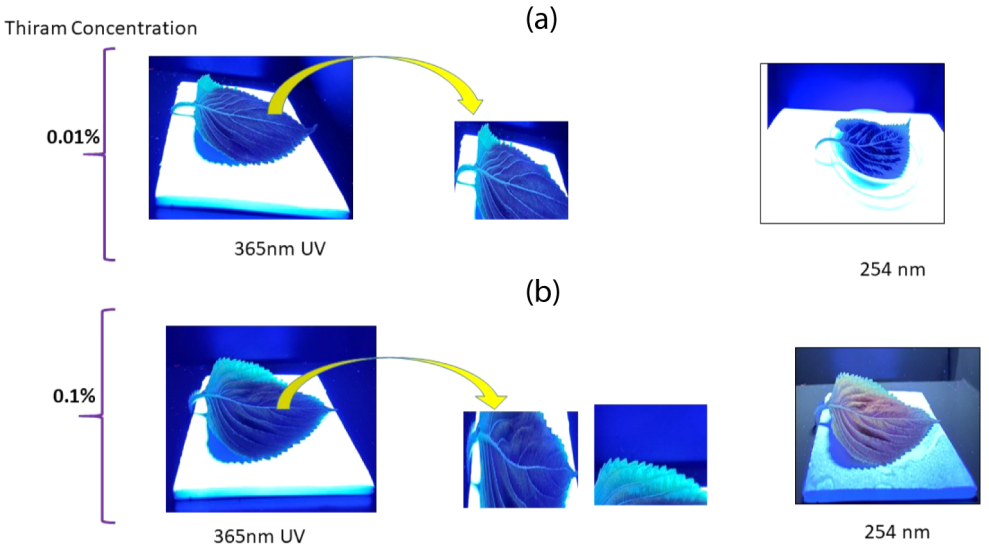

Figure 14. Visual appearance of doped CD (carbon dots) sprayed perilla leaves with (a) 0.01% thiram and (b) 0.1% thiram under both 365 and 254 nm UV light.

perilla leaves. The polynomial curve fitting method was employed to solve this issue because of its quick processing speed and simplicity compared to other fluorescence correction methods, such as wavelet transformation and Fourier transformation.[73,74] The primary principle of the polynomial curve approach is the use of iterative calculations to establish the correct polynomial arrangement. The polynomial curve fitting method has been applied in a number of previous studies in combination with Raman spectroscopy with better outcomes in a variety of areas, including the prediction of cucumber seed germination,[74] the determination of the quality of Grignard Reagent,[75] and the crude protein and oil content of soybeans.[73] The fluorescence-affected and polynomial-corrected Raman spectra are shown in Figure 12a,b. In this study, an eighth order polynomial with 100 iterations was selected.

Several undesirable effects, such as background noise, instrumental drifts, and scattering effects, are frequently present in the Raman spectrum data. These factors are directly related to the decline in model performances. Pretreatment techniques are therefore necessary in order to eliminate undesired scattering and noise effects from the spectrum data acquired with the use of a Raman spectrometer. In this study seven different kinds of preprocessing techniques which includes normalization (range, mean, and max), multiplicative signal correction (MSC), standard normal variate (SNV), and

https://doi.org/10.1021/acsomega.4c07090
ACS Omega 2024, 9, 47647−47660

first and second Savitzky−Golay (SG) derivatives were employed in this study for model performance enhancement. For more theoretical details, associated with the preprocessing techniques, following article is very useful.[76] After the preprocessing steps were performed, PLS-DA machine learning models were generated by using MATLAB version 7.0.4 (Math Works, Inc., MA, USA) software.

3.6. Visual Inspection of Perilla Leaves Infected with Thiram Insecticide and Sprayed with HSCDs and Their Spectral Interpretation. To investigate the presence of thiram pesticide on the perilla leaf, Figure 13a, two different concentrations, i.e., 0.01% and 0.1% were sprayed to the surface of perilla leaves as shown in Figure 13b,c. Following a 10 to 15 min intervals, HSCDs were likewise sprayed onto two distinct concentrations of perilla leaves infected with thiram. seen in Figure 13d,e. For ten hours, the leaves were kept at room temperature inside a chemical cabinet in order to ensure that thiram and HSCDs were distributed equally. The HSCDs could detect thiram insecticides in perilla leaves at both lower and higher concentrations, as Figure 13f,g demonstrates. There was a noticeable change on the surface of both leaves, and their Raman spectra were obtained. The SNV preprocessed Raman spectra are shown in Figure 13h, where they have been displayed between the 400−1800 cm^{-1} spectral range. Specific spectrum changes that were sensitive to thiram were observed in all four spectral peaks associated with the doped and nondoped CDs samples, which were sprayed on perilla leaves infected with two different doses. Blue, green, and red highlights are used to indicate the spectral fingerprints for thiram, which were detected at Raman shift values of 560, 1140−1150, and 1365−1380 cm^{-1}. These peaks are characteristic of thiram,[77,78] as per earlier research. Figure 14 shows that researchers have confirmed the infusion of carbon dots into the leaf parts. When the leaves are observed under 254 and 365 nm UV light, the veins, stalk, and superficial hairs emit blue fluorescence, indicating that the CDs have successfully traveled through the leaf tissue.

3.7. PLS-DA Classification Analysis for Raman Spectroscopy. The PLS-DA model was developed using 800 samples in total. A 70:30 split of the data was made into calibration and validation groups, with 300 samples in the validation set and 500 samples in the training or calibration set. A thorough summary of the data sets utilized to build the models is provided in Table 2.

Table 2. Datasets Used to Create Classification Model

Techniques	Model	Total samples	Calibration	Validation
Raman spectroscopy	PLS-DA	800	500	300

3.8. Partial Least Squares Discriminant Analysis (PLS-DA) for the Perilla Leaves Samples Spiked with Thiram Insecticide. The raw Raman spectrometer data of the pesticide-contaminated perilla leaves collected during the experiment cannot be used for classification analysis because they generate a lot of spectral attributes, all of which contribute to the declining classification performances. An essential method for identifying patterns and interpreting data is the PLS-DA algorithm. Additionally, the PLS-DA method is intended to handle complicated data sets more effectively than other traditional strategies by further dividing the groups. Furthermore, because it removes unnecessary variables while maintaining crucial information, PLS-DA is also a useful technique for dimension reduction. Through the preservation of significant characteristics, PLS-DA contributes to better data management. Previous research has demonstrated the PLS-DA algorithm's greater potential for classification analysis in various areas including agriculture,[79,80] food items,[81−84] and pharmaceuticals.[85−87] In this work, a discriminant analysis model was developed utilizing the PLS-DA machine learning approach to distinguish between doped and nondoped perilla leaf samples that were infected with thiram at two different concentrations. The classification plots for both data sets (calibration and validation) for 0.01% and 0.1% thiram insecticide concentrations on perilla leaves samples that were sprayed with doped and nondoped carbon dots samples are shown in Figure 15a−d, respectively. In both the calibration and validation plots for both groups of samples, there was a definite distinction between the two groups, yielding a classification accuracy of 100% in each case. SNV had the highest overall accuracy of 100% for the 0.01% and 0.1% concentration perilla samples, as shown in Table 3. This excellent classification accuracy demonstrates that the PLS-DA model has tremendous promise for classifying doped and nondoped CDs samples when used in conjunction with an adequate preprocessing technique.

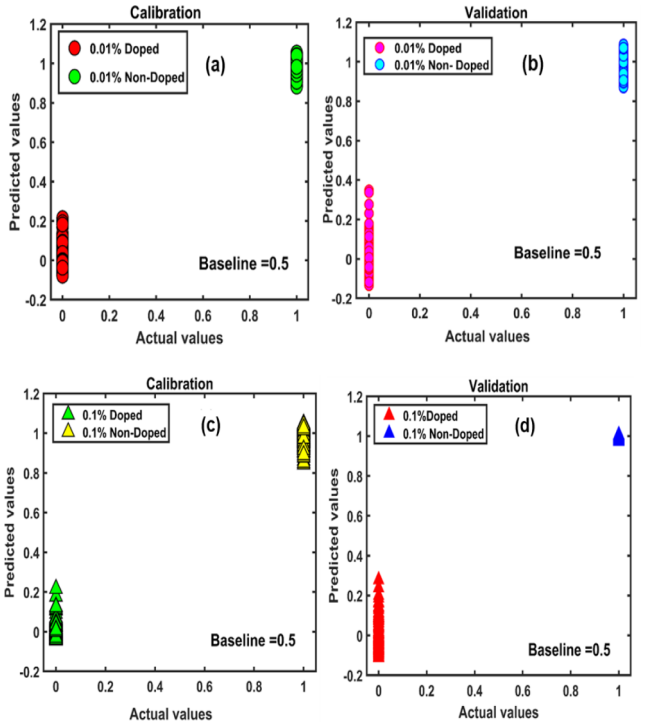

Figure 15. PLS-DA classification plots for (a) calibration and (b) validation for 0.01% HSCDs and HCDs thiram infected Perilla leaves. (c) Calibration and (d) validation for 0.1% HSCDs and HCDs thiram infected Perilla leaves using Raman spectroscopy. HCD, non-doped carbon dots; HSCD, doped carbon dots; PLS-DA, partial least-squares discriminant analysis.

In the past, pesticide detection in food samples has previously been performed with superior sensitivity and effectiveness using carbon dots with an excellent limit of detection (LOD) of 8 nM.[88] Another study used green carbon dots to detect ultrasensitive fluorescent pesticides in real samples, with detection limits of 0.25, 0.5, and 2 ng mL^{-1} for

https://doi.org/10.1021/acsomega.4c07090
ACS Omega 2024, 9, 47647−47660

Table 3. PLS-DA Classification Outcomes for 0.01, and 0.1% Thiram Infected Perilla Leaves Utilizing Raman Spectroscopy[a]

Samples	Calibration (n = 500)		Calibration Accuracy	Validation (n = 300)		Validation Accuracy	Total (n = 800)		Overall Accuracy
	True	False	Accuracy (%)	True	False	Accuracy (%)	True	False	Accuracy (%)
0.01%	500	0	100%	300	0	100%	800	0	100%
0.1%	500	0	100%	300	0	100%	800	0	100%

[a]PLS-DA, partial least-squares discriminant analysis.

diazinon, amicarbazone, and glyphosate, respectively.[31] We were unable to accomplish such LOD values in our investigation, but we intend to attempt them further in future investigations. However, the pesticides detection was also routinely carried out using conventional chromatography based approaches like high performance liquid chromatography,[89] liquid chromatography−mass spectrometry.[90] Conversely, carbon dots are preferable in terms of easy sample preparation, affordability, environmental friendliness, and ease of use. Additionally, multiple investigations employed FT-IR[91] and FT-NIR[92] spectroscopies for nondestructive testing of pesticides with better performance. However, moisture problems, overtone production, and combination bands frequently affect both spectroscopic approaches. In this study, we used Raman spectroscopy—which is excellent for handling samples of aqueous solutions and yields sharp, well-defined peaks free from the influence of combination bands and overtones—to examine the sensitivity of our produced fluorescent carbon dots for thiram pesticides. The detection and visualization of thiram insecticides on edible perilla leaves using our CDs, as a result, demonstrated that the limitations of the previously mentioned destructive chemical-based approaches as well as FT-IR and FT-NIR spectroscopic methods were successfully resolved in this present investigation.

4. CONCLUSIONS

In summary, we utilized environmentally friendly carbon dots derived from hibiscus petal powder, synthesized using a hydrothermal reaction, as fluorescent probes for the effective detection of pesticides. The carbon dots had active amino groups on their external surface along with less active carboxyl and hydroxyl groups. The interaction between carbon dots and target pesticides is primarily driven by the formation of a ground-state complex involving amino groups. In an aqueous solution, carbon dots remain in a clustered state because of hydrogen bonding and ionic interactions. Our zeta potential analysis indicated that the L-cysteine-modified carbon dots (HSCDs) were more stable and had a negative surface charge of −21 mV as compared to HCDs with −2 mV surface charge. The *QY* achieved for HCDs and HSCDs are 30% and 22% respectively. We observed that quenched PL is prominent in L-cysteine-modified carbon dots and the intensity was in the lower range for HSCDs. The reason we explained is due to protonation and deprotonation of electrons. However, not all surface functionalities were involved in self-complexation. The surface morphologies and elemental compositions of HCDs and HSCDs showed noticeable differences. The EDS analysis revealed that the HSCDs had a higher sulfur content, indicating successful doping of the carbon dots. Additionally, an intriguing aspect of the morphology was observed, suggesting that quantum wire confinement could be a potential feature in both types of carbon dots. Further, Raman spectral analysis revealed that different concentrations of thiram detected by HSCDs and HCDs have the potential to aid in the development of a straightforward, highly responsive, carefully chosen, measurable, environmentally conscious, and biologically compatible nanosensing approach. The presence of carbon dots within the leaf tissue was confirmed by the blue fluorescence observed in the leaf veins and stalks when exposed to UV light at 254 and 365 nm, as previously discussed.

In addition, the created PLS-DA machine learning models were able to distinguish between higher and lower amounts of thiram in perilla leaves for HCDs and HSCDs samples, with 100% classification accuracy for calibration and validation data sets. This method can be used in broader applications, particularly in the realm of agricultural sciences, to combat environmental pollution and minimize adverse impacts on human health.

AUTHOR INFORMATION

Corresponding Author

Byoung-Kwan Cho − *Department of Biosystems Machinery Engineering, Chungnam National University, Daejeon 34134, Republic of Korea; Department of Smart Agriculture Systems, College of Agricultural and Life Science, Chungnam National University, Daejeon 34134, Republic of Korea;* orcid.org/0000-0002-8397-9853; Email: chobk@cnu.ac.kr

Authors

Tanima Bhattacharya − *Department of Biosystems Machinery Engineering, Chungnam National University, Daejeon 34134, Republic of Korea; Faculty of Applied Science, Lincoln University College, Petaling Jaya, Selangor 47301, Malaysia*

Rahul Joshi − *Department of Biosystems Machinery Engineering, Chungnam National University, Daejeon 34134, Republic of Korea*

Lemma Teshome Tufa − *Institute of Materials Chemistry, Chungnam National University, Daejeon 34134, South Korea; Department of Chemistry, Adama Science and Technology University, P.O. Box 1888 Adama, Ethiopia;* orcid.org/0000-0001-6929-8464

Mahendra Goddati − *Department of Chemistry, Chemical Engineering and Applied Chemistry, Chungnam National University, Daejeon 34134, Republic of Korea;* orcid.org/0000-0003-2743-1954

Jaebeom Lee − *Department of Chemistry, Chemical Engineering and Applied Chemistry, Chungnam National University, Daejeon 34134, Republic of Korea;* orcid.org/0000-0002-8414-7290

Ameeta Tewari − *Department of Chemistry, M.B.G.P.G College Haldwani, Kumaun University, Nainital, Uttarakhand 263139, India*

Complete contact information is available at: https://pubs.acs.org/10.1021/acsomega.4c07090

Author Contributions

○T.B. and R.J. contributed equally to this work.

Notes

The authors declare no competing financial interest.

https://doi.org/10.1021/acsomega.4c07090
ACS Omega 2024, 9, 47647−47660

■ ACKNOWLEDGMENTS

The authors acknowledge supports from the BK21 FOUR Project for Smart Agriculture Systems, Chungnam National University, Republic of Korea.

■ REFERENCES

(1) Liu, J.; Li, R.; Yang, B. Carbon Dots: A New Type of Carbon-Based Nanomaterial with Wide Applications. *ACS Cent. Sci.* **2020**, *6* (12), 2179−2195.
(2) El-Shafey, A. M. Carbon Dots: Discovery, Structure, Fluorescent Properties, and Applications. *Green Process. Synth.* **2021**, *10* (1), 134−156.
(3) Khan, A.; Priyadarshi, R.; Bhattacharya, T.; Rhim, J. W. Carrageenan/Alginate-Based Functional Films Incorporated with Allium Sativum Carbon Dots for UV-Barrier Food Packaging. *Food Bioprocess Technol.* **2023**, *16*, 2001−2015.
(4) Reyes, D.; Camacho, M.; Camacho, M.; Mayorga, M.; Weathers, D.; Salamo, G.; Wang, Z.; Neogi, A. Laser Ablated Carbon Nanodots for Light Emission. *Nanoscale Res. Lett.* **2016**, *11* (1), 424.
(5) Shibata, H.; Abe, M.; Sato, K.; Uwai, K.; Tokuraku, K.; Iimori, T. Microwave-Assisted Synthesis and Formation Mechanism of Fluorescent Carbon Dots from Starch. *Carbohydr. Polym. Technol. Appl.* **2022**, *3*, 100218.
(6) Ouadi, M.; Bashir, M. A.; Speranza, L. G.; Jahangiri, H.; Hornung, A. Food and Market Waste-A Pathway to Sustainable Fuels and Waste Valorization. *Energy Fuels* **2019**, *33* (10), 9843−9850.
(7) Khan, A.; Ezati, P.; Rhim, J.-W.; Kim, J. T.; Molaei, R. Colloids Surfaces A Physicochem. Eng. Asp. PH-Sensitive Green Tea-Derived Carbon Quantum Dots for Real-Time Monitoring of Shrimp Freshness. *Colloids Surf., A* **2023**, *666*, 131242.
(8) Hu, Y.; Zhang, L.; Li, X.; Liu, R.; Lin, L.; Zhao, S. Green Preparation of S and N Co-Doped Carbon Dots from Water Chestnut and Onion as Well as Their Use as an Off−On Fluorescent Probe for the Quantification and Imaging of Coenzyme A. *ACS Sustainable Chem. Eng.* **2017**, *5* (6), 4992−5000.
(9) Sachdev, A.; Gopinath, P. Green Synthesis of Multifunctional Carbon Dots from Coriander Leaves and Their Potential Application as Antioxidants, Sensors and Bioimaging Agents. *Analyst* **2015**, *140* (12), 4260−4269.
(10) Tyagi, A.; Tripathi, K. M.; Singh, N.; Choudhary, S.; Gupta, R. K. Green Synthesis of Carbon Quantum Dots from Lemon Peel Waste: Applications in Sensing and Photocatalysis. *RSC Adv.* **2016**, *6* (76), 72423−72432.
(11) Pires, N. R.; Santos, C. M. W.; Sousa, R. R.; De Paula, R. C. M.; Cunha, P. L. R.; Feitosa, J. P. A. Novel and Fast Microwave-Assisted Synthesis of Carbon Quantum Dots from Raw Cashew Gum. *J. Braz. Chem. Soc.* **2015**, *26* (6), 1274−1282.
(12) Yang, X.; Zhuo, Y.; Zhu, S.; Luo, Y.; Feng, Y.; Dou, Y. Novel and Green Synthesis of High-Fluorescent Carbon Dots Originated from Honey for Sensing and Imaging. *Biosens. Bioelectron.* **2014**, *60*, 292−298.
(13) Sahu, S.; Behera, B.; Maiti, T. K.; Mohapatra, S. Simple One-Step Synthesis of Highly Luminescent Carbon Dots from Orange Juice: Application as Excellent Bio-Imaging Agents. *Chem. Commun.* **2012**, *48* (70), 8835−8837.
(14) Karaman, C. Orange Peel Derived-Nitrogen and Sulfur Co-doped Carbon Dots: A Nano-booster for Enhancing ORR Electrocatalytic Performance of 3D Graphene Networks. *Electroanalysis* **2021**, *33* (5), 1356−1369.
(15) Liu, W.; Diao, H.; Chang, H.; Wang, H.; Li, T.; Wei, W. Green Synthesis of Carbon Dots from Rose-Heart Radish and Application for Fe3+ Detection and Cell Imaging. *Sens. Actuators, B* **2017**, *241*, 190−198.
(16) Zhang, Z.; Sun, W.; Wu, P. Highly Photoluminescent Carbon Dots Derived from Egg White: Facile and Green Synthesis, Photoluminescence Properties, and Multiple Applications. *ACS Sustainable Chem. Eng.* **2015**, *3* (7), 1412−1418.
(17) Guo, Y.; Li, T.; Xie, L.; Tong, X.; Tang, C.; Shi, S. Red Pitaya Peels-Based Carbon Dots for Real-Time Fluorometric and Colorimetric Assay of Au3+, Cellular Imaging, and Antioxidant Activity. *Anal. Bioanal. Chem.* **2021**, *413* (3), 935−943.
(18) Shabbir, H.; Wojtaszek, K.; Rutkowski, B.; Csap, E.; Bednarski, M.; Adamiec, A.; Lutwin, M. G.; Mordyl, B.; Druciarek, J.; Kotańska, M.; et al. Milk - Derived Carbon Quantum Dots: Study of Biological and Chemical Properties Provides Evidence of Toxicity. *Molecules* **2022**, *27*, 8728.
(19) Borna, S.; Sabzi, R. E.; Pirsa, S. Synthesis of Carbon Quantum Dots from Apple Juice and Graphite: Investigation of Fluorescence and Structural Properties and Use as an Electrochemical Sensor for Measuring Letrozole. *J. Mater. Sci.: Mater. Electron.* **2021**, *32* (8), 10866−10879.
(20) Atchudan, R.; Jebakumar Immanuel Edison, T. N.; Shanmugam, M.; Perumal, S.; Somanathan, T.; Lee, Y. R. Sustainable Synthesis of Carbon Quantum Dots from Banana Peel Waste Using Hydrothermal Process for in Vivo Bioimaging. *Phys. E* **2021**, *126*, 114417.
(21) Vandarkuzhali, S. A. A.; Natarajan, S.; Jeyabalan, S.; Sivaraman, G.; Singaravadivel, S.; Muthusubramanian, S.; Viswanathan, B. Pineapple Peel-Derived Carbon Dots: Applications as Sensor, Molecular Keypad Lock, and Memory Device. *ACS Omega* **2018**, *3* (10), 12584−12592.
(22) Murugan, R. V.; Sridharan, G.; Atchudan, R.; Arya, S.; Ganapathy, D.; Sundramoorthy, A. Fluorometric Determination of Fe3+ Ions Using Green Synthesized Carbon Quantum Dots from Damask Rose Flowers. *Curr. Nanosci.* **2024**, 1−11.
(23) Rojas-Valencia, O. G.; Regules-Carrasco, M.; Hernández-Fuentes, J.; Germán, C. M. R.-S.; Estrada-Flores, M.; Villagarcía-Chávez, E. Synthesis of Blue Emissive Carbon Quantum Dots from Hibiscus Sabdariffa Flower: Surface Functionalization Analysis by FT-IR Spectroscopy. *Materialia* **2021**, *19* (August), 101182.
(24) Rani, N.; Ali, F.; Muhammad, M.; AlOthman, Z. A. Development of Fluorescent Co (II)-Integrated Carbon Dots and Their Application as a Off-On Mesotrione Detection Sensor. *ACS Omega* **2023**, *8* (51), 49115−49128.
(25) Wang, C.; Xu, J.; Zhang, R.; Zhao, W. Facile and Low-Energy-Consumption Synthesis of Dual-Functional Carbon Dots from Cornus Walteri Leaves for Detection of p-Nitrophenol and Photocatalytic Degradation of Dyes. *Colloids Surf., A* **2022**, *640*, 128351.
(26) Gaviria, M. I.; Barrientos, K.; Arango, J. P.; Cano, J. B.; Peñuela, G. A. Highly Sensitive Fluorescent Biosensor Based on Acetylcholinesterase and Carbon Dots−Graphene Oxide Quenching Test for Analytical and Commercial Organophosphate Pesticide Detection. *Front. Environ. Sci.* **2022**, *10* (March), 1−13.
(27) Ullal, N.; Muthamma, K.; Sunil, D. Carbon Dots from Eco-Friendly Precursors for Optical Sensing Application: An up-to-Date Review. *Versita* **2022**, *76*, 6097.
(28) Zhang, X.; Liao, X.; Hou, Y.; Jia, B.; Fu, L.; Jia, M.; Zhou, L.; Lu, J.; Kong, W. Recent Advances in Synthesis and Modification of Carbon Dots for Optical Sensing of Pesticides. *J. Hazard. Mater.* **2022**, *422*, 126881.
(29) Zhang, Y.; Zhao, J.; Sun, X.; Pan, W.; Yu, G.; Wang, J. Fluorescent Carbon Dots for Probing the Effect of Thiram on the Membrane of Fungal Cell and Its Quantitative Detection in Aqueous Solution. *Sens. Actuators, B* **2018**, *273*, 1833−1842.
(30) Landa, S. D. T.; Bogireddy, N. K.; Kaur, I.; Batra, V.; Agarwal, V. IScience Ll Heavy Metal Ion Detection Using Green Precursor Derived Carbon Dots. *iScience* **2022**, *25* (2), 103816.
(31) Ashrafi Tafreshi, F.; Fatahi, Z.; Ghasemi, S. F.; Taherian, A.; Esfandiari, N. Ultrasensitive Fluorescent Detection of Pesticides in Real Sample by Using Green Carbon Dots. *PLoS One* **2020**, *15* (3), No. e0230646.
(32) Cho, J.; Sa, K. J.; Park, H.; Heo, T. H.; Lee, S.; Lee, J. K. Heliyon Association Analysis of Leaf Aromatic Substances in Cultivated and Weedy Types of Perilla Crop Using SSR Markers. *Heliyon* **2024**, *10* (15), No. e34995.

https://doi.org/10.1021/acsomega.4c07090
ACS Omega 2024, 9, 47647−47660

(33) Sardar, S. W.; Byeon, G. D.; Choi, J. Y.; Ham, H. J.; Ishag, A. E. S. A.; Hur, J. H. Residual Characteristics and Safety Assessment of the Insecticides Spiromesifen and Chromafenozide in Lettuce and Perilla. *Sci. Rep.* **2022**, *12* (1), 1−9.
(34) Igarashi, M.; Miyazaki, Y.A Review on Bioactivities of Perilla: Progress in Research on the Functions of Perilla as Medicine and Food*Evidence-Based Complementary and Alternative Medicine*201320139925342
(35) Wu, X.; Dong, S.; Chen, H.; Guo, M.; Sun, Z.; Luo, H. Perilla Frutescens: A Traditional Medicine and Food Homologous Plant. *Chinese Herb. Med.* **2023**, *15* (3), 369−375.
(36) Mungmai, L.; Preedalikit, W.; Aunsri, N.; Amornlerdpison, D. Efficacy of Cosmetic Formulation Containing Perilla Frutescens Leaves Extract for Irritation and Aging Skin. *Biomed. Pharmacol. J.* **2020**, *13* (2), 779−787.
(37) Vedernikova, A. A.; Miruschenko, M. D.; Arefina, I. A.; Xie, J.; Huang, H.; Koroleva, A. V.; Zhizhin, E. V.; Cherevkov, S. A.; Timin, A. S.; Mitusova, K. A.; Shipilovskikh, S. A.; Ushakova, E. V. Green and Red Emissive N,O-Doped Chiral Carbon Dots Functionalized with l-Cysteine. *J. Phys. Chem. Lett.* **2024**, *15* (1), 113−120.
(38) Suner, S. S.; Sahiner, M.; Ayyala, R. S.; Bhethanabotla, V. R.; Sahiner, N. Versatile Fluorescent Carbon Dots from Citric Acid and Cysteine with Antimicrobial, Anti-Biofilm, Antioxidant, and AChE Enzyme Inhibition Capabilities. *J. Fluoresc.* **2021**, *31* (6), 1705−1717.
(39) Muro-Hidalgo, J. M.; Bazany-Rodríguez, I. J.; Hernández, J. G.; Pabello, V. M. L.; Thangarasu, P. Histamine Recognition by Carbon Dots from Plastic Waste and Development of Cellular Imaging: Experimental and Theoretical Studies. *J. Fluoresc.* **2023**, *33* (5), 2041−2059.
(40) Tafreshi, F. A.; Fatahi, Z.; Ghasemi, S. F.; Taherian, A.; Esfandiari, N. Ultrasensitive Fluorescent Detection of Pesticides in Real Sample by Using Green Carbon Dots. *PLoS One* **2020**, *15* (3), No. e0230646.
(41) Atchudan, R.; Edison, T. N. J. I.; Perumal, S.; Muthuchamy, N.; Lee, Y. R. Hydrophilic Nitrogen-Doped Carbon Dots from Biowaste Using Dwarf Banana Peel for Environmental and Biological Applications. *Fuel* **2020**, *275*, 117821.
(42) Sarkar, T.; Bohidar, H. B.; Solanki, P. R. Carbon Dots-Modified Chitosan Based Electrochemical Biosensing Platform for Detection of Vitamin D. *Int. J. Biol. Macromol.* **2018**, *109*, 687−697.
(43) Cao, L.; Zan, M.; Chen, F.; Kou, X.; Liu, Y.; Wang, P.; Mei, Q.; Hou, Z.; Dong, W.-F.; Li, L. Formation Mechanism of Carbon Dots: From Chemical Structures to Fluorescent Behaviors. *Carbon* **2022**, *194*, 42−51.
(44) Bhattacharya, T.; Do, H. A.; Rhim, J. W.; Shin, G. H.; Kim, J. T. Facile Synthesis of Multifunctional Carbon Dots from Spent Gromwell Roots and Their Application as Coating Agents. *Foods* **2023**, *12* (11), 2165.
(45) Barker, M.; Rayens, W. Partial Least Squares for Discrimination. *J. Chemom.* **2003**, *17*, 166−173.
(46) Kandpal, L. M.; Lee, S.; Kim, M. S.; Bae, H.; Cho, B.-K. Short Wave Infrared (SWIR) Hyperspectral Imaging Technique for Examination of Aflatoxin B1 (AFB1) on Corn Kernels. *Food Control* **2015**, *51*, 171−176.
(47) Sharma, V.; Singh, S. K.; Mobin, S. M. Bioinspired Carbon Dots: From Rose Petals to Tunable Emissive Nanodots. *Nanoscale Adv.* **2019**, *1* (4), 1290−1296.
(48) Yalshetti, S.; Thokchom, B.; Bhavi, S. M.; Singh, S. R.; Patil, S. R.; Harini, B. P.; Sillanpää, M.; Manjunatha, J. G.; Srinath, B. S.; Yarajarla, R. B. Microwave-Assisted Synthesis Characterization and in Vitro Biomedical Applications of Hibiscus Rosa-Sinensis Linn.-Mediated Carbon Quantum Dots. *Sci. Rep.* **2024**, *14* (1), 1−13.
(49) Bala, R.; Kaur, R.; Kaur, B.; Kaur, P. Hibiscus Rosa Sinensis Linn. *Int. J. Health Sci.* **2022**, *6* (March), 5165−5193.
(50) Bao, H.; Liu, Y.; Li, H.; Qi, W.; Sun, K. Luminescence of Carbon Quantum Dots and Their Application in Biochemistry. *Heliyon* **2023**, *9* (10), No. e20317.
(51) Wu, W.; Zhan, L.; Fan, W.; Song, J.; Li, X.; Li, Z.; Wang, R.; Zhang, J.; Zheng, J.; Wu, M.; Zeng, H. Cu-N Dopants Boost Electron Transfer and Photooxidation Reactions of Carbon Dots. *Angew. Chem., Int. Ed.* **2015**, *54* (22), 6540−6544.
(52) Atchudan, R.; Chandra Kishore, S.; Gangadaran, P.; Jebakumar Immanuel Edison, T. N.; Perumal, S.; Rajendran, R. L.; Alagan, M.; Al-Rashed, S.; Ahn, B. C.; Lee, Y. R. Tunable Fluorescent Carbon Dots from Biowaste as Fluorescence Ink and Imaging Human Normal and Cancer Cells. *Environ. Res.* **2022**, *204* (PD), 112365.
(53) Yang, Y.; Sreekumar, S.; Chimenti, R. V.; Veksler, M.; Song, K.; Zhang, S.; Rodas, D.; Christianson, V.; O'Carroll, D. M. Polypropylene-Derived Luminescent Carbon Dots. *ACS Mater. Lett.* **2024**, *6* (5), 1968−1976.
(54) Kumar, V. B.; Mirsky, S. K.; Shaked, N. T.; Gazit, E. High Quantum Yield Amino Acid Carbon Quantum Dots with Unparalleled Refractive Index. *ACS Nano* **2024**, *18* (3), 2421−2433.
(55) Pandiyan, S.; Arumugam, L.; Srirengan, S. P.; Pitchan, R.; Sevugan, P.; Kannan, K.; Pitchan, G.; Hegde, T. A.; Gandhirajan, V. Biocompatible Carbon Quantum Dots Derived from Sugarcane Industrial Wastes for Effective Nonlinear Optical Behavior and Antimicrobial Activity Applications. *ACS Omega* **2020**, *5* (47), 30363−30372.
(56) Anpalagan, K.; Yin, H.; Cole, I.; Zhang, T.; Lai, D. T. H. Quantum Yield Enhancement of Carbon Quantum Dots Using Chemical-Free Precursors for Sensing Cr (VI) Ions. *Inorganics* **2024**, *12* (4), 96.
(57) Kamble, P.; Malavekar, D.; Tiwari, A. P. Natural Biowaste Derived Fluorescent Carbon Quantum Dots: Synthesis, Characterization and Biocompatibility Study. *J. Fluoresc.* **2024**, *34* (1), 191−201.
(58) Ren, H.; Chen, Y.; Labidi, A.; Zhao, K.; Xu, X.; Othman, S. I.; Allam, A. A.; Rudayni, H. A.; Wang, C. Transforming Bio-Waste Lignin into Amine Functionalized Carbon Quantum Dots for Selective Detection of Trace Cu2+ in Aqueous System. *Int. J. Biol. Macromol.* **2024**, *273*, 133118.
(59) Zhou, C.; Wu, S.; Qi, S.; Song, W.; Sun, C. Facile and High-Yield Synthesis of N-Doped Carbon Quantum Dots from Biomass Quinoa Saponin for the Detection of Co2+. *J. Anal. Methods Chem.* **2021**, *2021* (1), 9732364.
(60) Jiao, X.-Y.; Li, L.; Qin, S.; Zhang, Y.; Huang, K.; Xu, L. The Synthesis of Fluorescent Carbon Dots from Mango Peel and Their Multiple Applications. *Colloids Surf., A* **2019**, *577*, 306−314.
(61) Devi, S.; Gupta, R. K.; Paul, A. K.; Tyagi, S. Waste Carbon Paper Derivatized Carbon Quantum Dots/(3-Aminopropyl)-Triethoxysilane Based Fluorescent Probe for Trinitrotoluene Detection. *Mater. Res. Express* **2019**, *6*, 025605.
(62) Surendran, P.; Lakshmanan, A.; Vinitha, G.; Ramalingam, G.; Rameshkumar, P. Facile Preparation of High Fluorescent Carbon Quantum Dots from Orange Waste Peels for Nonlinear Optical Applications. *Luminescence* **2020**, *35* (2), 196−202.
(63) Mohandoss, S.; Ahmad, N.; Velu, K. S.; Khan, M. R.; Palanisamy, S.; You, S.; Lee, Y. R. Synthesis of Photoluminescent Carbon Dots Using Hibiscus Tea Waste and Heteroatom Doping for Multi-Metal Ion Sensing: Applications in Cell Imaging and Environmental Samples. *Chemosensors* **2023**, *11*, 474.
(64) Zou, S.; Hou, C.; Fa, H.; Zhang, L.; Ma, Y.; Dong, L.; Li, D.; Huo, D.; Yang, M. An Efficient Fluorescent Probe for Fluazinam Using N, S Co-Doped Carbon Dots from l-Cysteine. *Sens. Actuators, B* **2017**, *239*, 1033−1041.
(65) Sanni, S. O.; Moundzounga, T. H. G.; Oseghe, E. O.; Haneklaus, N. H.; Viljoen, E. L.; Brink, H. G. One-Step Green Synthesis of Water-Soluble Fluorescent Carbon Dots and Its Application in the Detection of Cu2+. *Nanomaterials* **2022**, *12* (6), 958.
(66) Martineau, S. Directed Diffusion-Limited Aggregation. *Alea* **2017**, *14* (1), 249−270.
(67) Zhang, B.; Ye, X.; Dai, W.; Hou, W.; Zuo, F.; Xie, Y. Biomolecule-Assisted Synthesis of Single-Crystalline Selenium Nanowires and Nanoribbons via a Novel Flake-Cracking Mechanism. *Nanotechnology* **2006**, *17* (2), 385.

https://doi.org/10.1021/acsomega.4c07090
ACS Omega 2024, 9, 47647−47660

(68) He, J.; Xiong, Y.; Mu, H.; Li, P.; Deng, Y.; Zou, W.; Zhao, Q. Antibacterial Properties of Three-Dimensional Flower Cluster ZIF-L Modified by N-Doped Carbon Dots. *Crystals* **2023**, *13* (4), 564.
(69) Hagiwara, K.; Horikoshi, S.; Serpone, N. Photoluminescent Carbon Quantum Dots: Synthetic Approaches and Photophysical Properties. *Chem. - Eur. J.* **2021**, *27* (37), 9466−9481.
(70) Yuan, F.; Yuan, T.; Sui, L.; Wang, Z.; Xi, Z.; Li, Y.; Li, X.; Fan, L.; Tan, Z.; Chen, A.; Jin, M.; Yang, S. Engineering Triangular Carbon Quantum Dots with Unprecedented Narrow Bandwidth Emission for Multicolored LEDs. *Nat. Commun.* **2018**, *9* (1), 1−11.
(71) Das, A.; Arefina, I. A.; Danilov, D. V.; Koroleva, A. V.; Zhizhin, E. V.; Parfenov, P. S.; Kuznetsova, V. A.; Ismagilov, A. O.; Litvin, A. P.; Fedorov, A. V.; Ushakova, E. V.; Rogach, A. L. Chiral Carbon Dots Based on l/d-Cysteine Produced: Via Room Temperature Surface Modification and One-Pot Carbonization. *Nanoscale* **2021**, *13* (17), 8058−8066.
(72) Mohammed, S. J.; Omer, K. M.; Hawaiz, F. E. Deep Insights to Explain the Mechanism of Carbon Dot Formation at Various Reaction Times Using the Hydrothermal Technique: FT-IR, 13C-NMR, 1H-NMR, and UV-Visible Spectroscopic Approaches. *RSC Adv.* **2023**, *13* (21), 14340−14349.
(73) Lee, H.; Cho, B.-K.; Kim, M. S.; Lee, W.-H.; Tewari, J.; Bae, H.; Sohn, S.-I.; Chi, H.-Y. Prediction of Crude Protein and Oil Content of Soybeans Using Raman Spectroscopy. *Sens. Actuators, B* **2013**, *185*, 694−700.
(74) Mo, C.; Kang, S.; Lee, K.; Kim, G.; Cho, B.-K.; Lim, J.-G.; Lee, H.-S.; Park, J. Germination Prediction of Cucumber (Cucumis Sativus) Seed Using Raman Spectroscopy. *J. Biosyst. Eng.* **2012**, *37* (6), 404−410.
(75) Joshi, R.; Joshi, R.; Mo, C.; Faqeerzada, M. A.; Amanah, H. Z.; Masithoh, R. E.; Kim, M. S.; Cho, B.-K. Raman Spectral Analysis for Quality Determination of Grignard Reagent. *Appl. Sci.* **2020**, *10* (10), 3545.
(76) Rinnan, Å.; Van Den Berg, F.; Engelsen, S. B. Review of the Most Common Pre-Processing Techniques for near-Infrared Spectra. *TrAC, Trends Anal. Chem.* **2009**, *28* (10), 1201−1222.
(77) Pu, H.; Huang, Z.; Xu, F.; Sun, D.-W. Two-Dimensional Self-Assembled Au-Ag Core-Shell Nanorods Nanoarray for Sensitive Detection of Thiram in Apple Using Surface-Enhanced Raman Spectroscopy. *Food Chem.* **2021**, *343*, 128548.
(78) Dao, T. C.; Luong, T. Q. N.; Cao, T. A.; Kieu, N. M. High-Sensitive SERS Detection of Thiram with Silver Nanodendrites Substrate. *Adv. Nat. Sci.: Nanosci. Nanotechnol.* **2019**, *10* (2), 025012.
(79) Yulia, M.; Suhandy, D. Authentication of Organic Lampung Robusta Ground Roasted Coffee by UV-Visible Spectroscopy and PLS-DA Method. *J. Phys.: Conf. Ser.* **2019**, *1341*, 022006.
(80) Neves, M. D. G.; Poppi, R. J.; Breitkreitz, M. C. Authentication of Plant-Based Protein Powders and Classification of Adulterants as Whey, Soy Protein, and Wheat Using FT-NIR in Tandem with OC-PLS and PLS-DA Models. *Food Control* **2022**, *132*, 108489.
(81) Joshi, R.; Adhikari, S.; Son, J. P.; Jang, Y.; Lee, D.; Cho, B.-K. Au Nanogap SERS Substrate for the Carbaryl Pesticide Determination in Juice and Milk Using Chemomterics. *Spectrochim. Acta, Part A* **2023**, *297*, 122734.
(82) Joshi, R.; Adhikari, S.; Kim, M.; Jang, Y.; Min, H. J.; Lee, D.; Cho, B.-K. Trace Level Detection of Melamine and Cyanuric Acid Extracted from Pet Liquid Food (Milk) Using a SERS Au Nanogap Substrate. *Curr. Res. Food Sci.* **2024**, *8*, 100726.
(83) Joshi, R.; Lohumi, S.; Joshi, R.; Kim, M. S.; Qin, J.; Baek, I.; Cho, B.-K. Raman Spectral Analysis for Non-Invasive Detection of External and Internal Parameters of Fake Eggs. *Sens. Actuators, B* **2020**, *303*, 127243.
(84) Adhikari, S.; Joshi, R.; Joshi, R.; Kim, M.; Jang, Y.; Tufa, L. T.; Gicha, B. B.; Lee, J.; Lee, D.; Cho, B.-K. Rapid and Ultrasensitive Detection of Thiram and Carbaryl Pesticide Residues in Fruit Juices Using SERS Coupled with the Chemometrics Technique. *Food Chem.* **2024**, *457*, 140486.
(85) Shahzad, K.; Nawaz, H.; Majeed, M. I.; Nazish, R.; Rashid, N.; Tariq, A.; Shakeel, S.; Shahzadi, A.; Yousaf, S.; Yaqoob, N. Classification of Tuberculosis by Surface-Enhanced Raman Spectroscopy (SERS) with Principal Component Analysis (PCA) and Partial Least Squares − Discriminant Analysis (PLS-DA). *Anal. Lett.* **2022**, *55* (11), 1731−1744.
(86) Grosso, R. A.; Walther, A. R.; Brunbech, E.; Sørensen, A.; Schebye, B.; Olsen, K. E.; Qu, H.; Hedegaard, M. A. B.; Arnspang, E. C. Detection of Low Numbers of Bacterial Cells in a Pharmaceutical Drug Product Using Raman Spectroscopy and PLS-DA Multivariate Analysis. *Analyst* **2022**, *147* (15), 3593−3603.
(87) Mansouri, M. A.; Ziemons, E.; Sacre, P.-Y.; Kharbach, M.; Barra, I.; Cherrah, Y.; Hubert, P.; Marini, R. D. Classification of Polymorphic Forms of Fluconazole in Pharmaceuticals by FT-IR and FT-NIR Spectroscopy. *J. Pharm. Biomed. Anal.* **2021**, *196*, 113922.
(88) Man, H.; Chaima, M.; Wang, X.; Xiu, L.; Yang, L.; Huang, J. Fluorescent Detection of Organophosphorus Pesticides Using Carbon Dots Derived from Broccoli. *Arab. J. Sci. Eng.* **2023**, *48* (7), 8315−8324.
(89) Gupta, B.; Rani, M.; Kumar, R. Degradation of Thiram in Water, Soil and Plants: A Study by High-performance Liquid Chromatography. *Biomed. Chromatogr.* **2012**, *26* (1), 69−75.
(90) Ringli, D.; Schwack, W. Selective Determination of Thiram Residues in Fruit and Vegetables by Hydrophilic Interaction LC-MS. *Food Addit. Contam.: Part A* **2013**, *30* (11), 1909−1917.
(91) Abdelgwad, M.; Tawfik, W.; Zedan, A.; Radwan, O. Determination of Saturated and Unsaturated Hydrocarbons in Petroleum Oil Pesticides Using FTIR Spectroscopy. *Egypt. J. Chem.* **2024**, *67* (2), 581−585.
(92) Lapcharoensuk, R.; Fhaykamta, C.; Anurak, W.; Chadwut, W.; Sitorus, A. Nondestructive Detection of Pesticide Residue (Chlorpyrifos) on Bok Choi (Brassica Rapa Subsp. Chinensis) Using a Portable NIR Spectrometer Coupled with a Machine Learning Approach. *Foods* **2023**, *12* (5), 955.

https://doi.org/10.1021/acsomega.4c07090
ACS Omega 2024, 9, 47647−47660